FATIGUE DAMAGE CHARACTERIZATION OF A TRI-AXIALLY BRAIDED POLYMER MATRIX COMPOSITE MATERIAL

J. Montesano[1*], Z. Fawaz[1], C. Poon[1], K. Behdinan[2]

[1]*Dept. of Aerospace Eng., Ryerson University, 350 Victoria St., Toronto, Canada M5B2K3*
[2]*Dept. of Mechanical & Ind. Eng., University of Toronto, 5 King's College Rd., Toronto, Canada M5S3G8*
**gmontesa@ryerson.ca*

Keywords: Braided polymeric composite, Fatigue, Experimental testing, Damage model.

Abstract
The focus of the study was to characterize and model fatigue damage for a tri-axially braided polymeric composite. Static tests revealed bilinear stress-strain behaviour, which was caused by saturation of braider yarn cracks. Utilization of edge replication and post mortem microscopy for cyclic test samples assisted in demonstrating that crack density correlated with the exhibited stiffness degradation. The corresponding analytical fatigue damage model accurately captured the damage development compared to the obtained experimental data.

1 Introduction

Advanced carbon fiber-reinforced polymer matrix composite (PMC) laminates have been more frequently employed for primary load bearing aerospace applications due to superior strength-to-weight and stiffness-to-weight ratios. Despite their considerable use in recent years, a number of manufacturing and performance disadvantages have been identified with PMC laminates. As a result the development of braided fabric-reinforced polymeric composite materials has significantly progressed. Braided fabric composites have many advantages compared to conventional laminates such as better overall through-the-thickness strength properties including superior impact damage resistance and delamination resistance, improved fatigue performance and lower notch sensitivity [1], [2]. In addition, manufacturing complex shaped parts using braided fabrics are easier and generally have lower associated costs due to the conformability of braided fabrics coupled with the use of a resin transfer molding (RTM) technique. The automated forming of textile fabrics further reduces manufacturing costs by eliminating tedious manual lay-up, which renders braided composites to be cost-competitive alternatives for component manufacturing.

In spite of the indicated advantages, the use of braided PMC materials is limited to only a few primary load bearing applications in the aerospace industry. There are few fatigue studies available in the open literature on braided composites which limits the available mechanical performance data. There are also few in-depth studies focused on fatigue damage of braided polymeric composites and the relationship between local damage and macroscopic material properties of these materials [3], [4]. The resulting microscopic damage behaviour of cyclically loaded braided polymeric composites is complex due to the local fiber architecture and additional geometric variables, which leads to distinct macroscopic behaviour which is

dependent on fabric architecture. A better understanding of the internal damage states is required to predict the fatigue behaviour of braided polymeric composites. It is therefore the objective of this study to characterize and subsequently model the fatigue damage of a tri-axially braided carbon fiber PMC material. The following sections outline the experimental details, present and discuss the experimental results, outline the developed analytical fatigue damage model and summarize the conclusions.

2 Experimental details

The material under investigation is a tri-axially braided fabric consisting of T650/35-6K carbon fiber yarns with a 0˚/±60˚ braid geometry embedded in a thermosetting polyimide resin. The warp fiber yarns (0˚) are ideally straight without any crimping, while the braider yarns (±60˚) are fabricated in a two-by-two braid pattern. The flat composite panels were manufactured by layering the two-dimensional braided fabric in a mold and using a RTM technique, resulting in a fiber volume fraction of 56%. All panels were inspected for manufacturing defects using a thru-transmission immersion ultrasonic c-scan method. For all panels, no visible defects were found. Each panel was cut along the warp direction using an abrasive waterjet cutting technique for test specimen manufacture. The nominal specimen dimensions were 355 mm x 25 mm, and were in accordance with ASTM 3479 test standard [5]. The edges of all cut specimens were subsequently wet sanded with 180-grit and then 320-grit paper for improved edge quality. All test specimens were equipped with 10˚ tapered aluminum end tabs to eliminate any potential issues with gripping induced failure.

All uniaxial tensile tests were conducted at room temperature on an MTS 322 test frame with hydraulically operated wedge grips. A surface mounted extensometer was used to monitor the specimen axial strain during static testing and the hysteretic material behaviour continuously throughout cycling. Edge replications were extracted for some of the test specimens using acetone and cellulose acetate film in order to track damage progression during loading. Scanning electron microscopy (SEM) was also utilized for additional damage observations *post mortem* after destructive sectioning of the test specimens. Ultimate static tests were conducted in displacement control with a constant crosshead speed of 2 mm/minute. Tension-tension fatigue tests were conducted in load control until specimen failure occurred using a constant amplitude sinusoidal waveform, a loading frequency of 5 Hz and a stress ratio of 0.1 at various maximum applied stress levels.

3 Experimental results and discussion

3.1 Static

In total five ultimate static tests were conducted to obtain the ultimate strength of the material and to characterize the damage mechanisms during quasi-static loading. A normalized stress-strain plot is shown in Figure 1, which illustrates the characteristic bilinear behaviour of the investigated braided composite. At the transition point, the effective material stiffness instantly drops by ~20%. This behaviour is analogous to that exhibited by some quasi-isotropic polymeric laminates loaded statically [6]. Edge replications were extracted during two additional static tests, which were conducted with the purpose of identifying the dominant damage modes and for determining the evolving crack density that resulted in the exhibited stress-strain behaviour. These tests were paused at various stress levels in a stepwise manner to extract the edge replications while the load was held constant. After pausing the tests, loading resumed with the same constant crosshead speed. The edge replications revealed that the dominant damage mode was transverse cracking in the braider yarns propagating along

the braider yarn axes in the ±60˚ specimen directions. There were few observed interface cracks between adjacent braider yarns or cracks in the matrix-rich zones. A plot of the crack density evolution is shown in Figure 2 (a). Two main observations are clear from the plot, mainly that the braider yarn crack density is far greater compared to the other observed damage modes and that there is a sudden increase in the number of braider yarn cracks as the applied stress reaches the transition stress (see vertical line in Figure 2 (a)). SEM observations confirmed that the majority of damage was in fact braider yarn cracking, where no damage was observed in the warp yarns as is shown in Figure 2 (b). From these observations it can be concluded that the crack density in the braider yarns rapidly increases once the transition stress is reached, causing the braider yarns to be less effective in carrying load as the applied stress increases further. As a result, load is transferred to the 0˚ fiber yarns which sustain more of the increasing load until local failure of these fiber yarns results in rapid failure of the specimen. This is the mechanism causing the instantaneous drop in stiffness at the bilinear transition point in the stress-strain plot, which is important for understanding the fatigue damage characteristics of this material as will be discussed in Section 3.2.

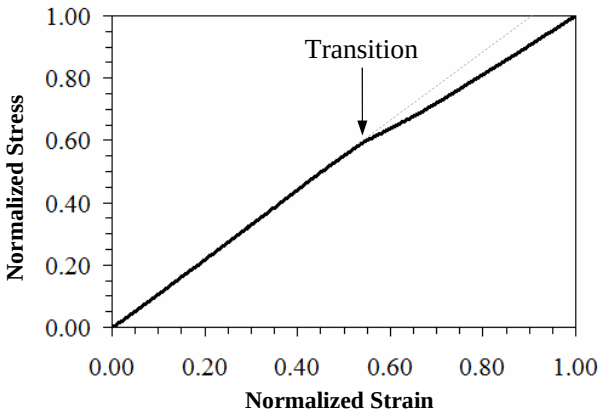

Figure 1. Ultimate static test normalized stress-strain plot (crosshead speed of 2 mm/min).

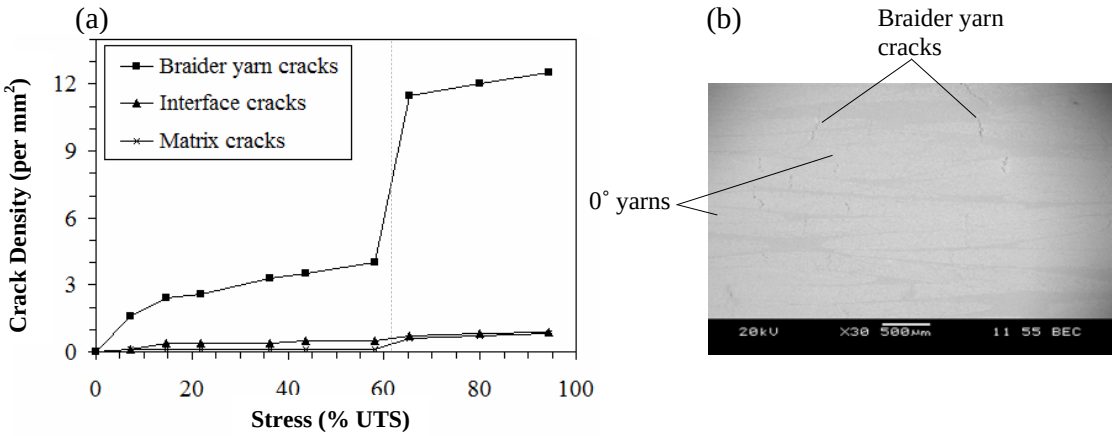

Figure 2. Ultimate static test (a) crack density evolution, (b) post mortem SEM photomicrograph.

3.2 Fatigue

A minimum of three fatigue tests were conducted at each maximum applied stress level for a number of stresses within the range of 50%-85% UTS. The corresponding stress-life (S-N)

curve for the braided composite is shown in Figure 3, where the average fatigue life values for each applied maximum stress are shown in the plot. The ordinate of the plot is the ratio of the maximum applied stress over the static ultimate tensile strength (S_{max}/S_u), while the abscissa is the number of cycles to failure (N_f) on a logarithmic scale. The data point on the ordinate corresponds to the static strength of the material. A run-off of 10^7 cycles was defined in this study as the test limit, which is indicated on the plot for stress levels of 50% and 60% UTS. A commonly employed semi-logarithmic relationship was found to fit the S-N data of Figure 3, which is defined in Equation 1. Data for the test samples that were cycled for 10^7 cycles without failure were not included in the regression that resulted in Equation 1.

$$\frac{S_{\max}}{S_u} = 1 - A\log\left(N_f\right) \tag{1}$$

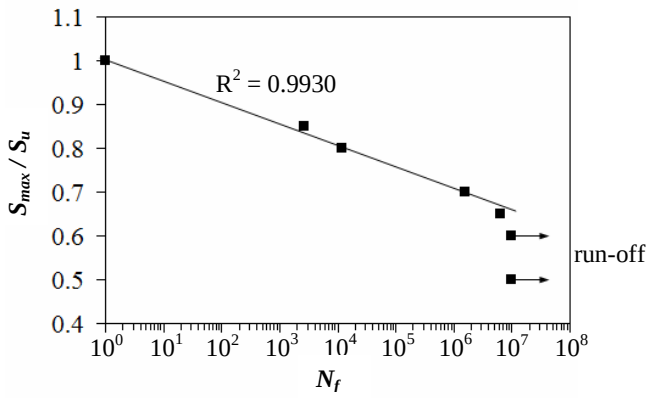

Figure 3. S-N curve, f = 5 Hz, R = 0.1.

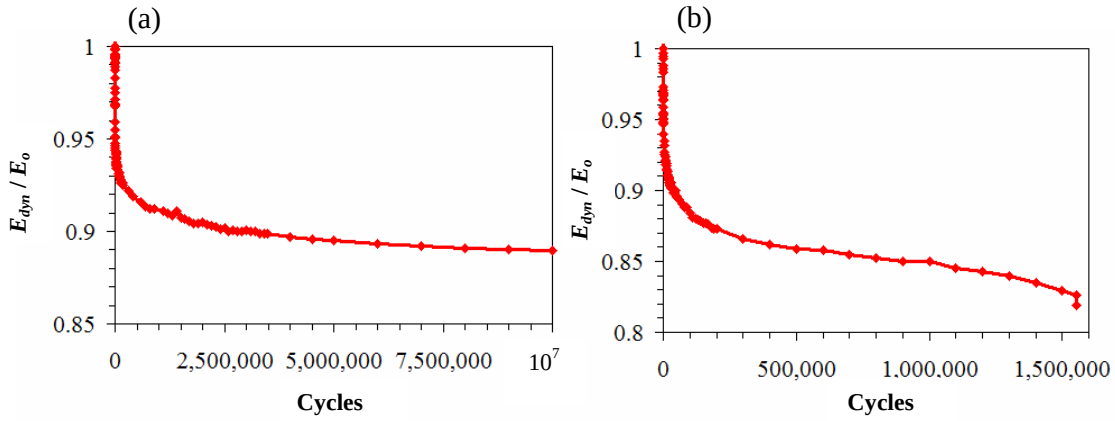

Figure 4. Stiffness degradation, f = 5 Hz, R = 0.1, maximum applied stress of (a) 50% UTS, (b) 70% UTS.

The obtained dynamic stiffness degradation profiles for 50% UTS and 70% UTS maximum applied stress cyclic tests are shown in Figure 4 (a) and (b), respectively. All samples cycled to failure exhibited a three-stage stiffness degradation profile. This was characterized by rapid stiffness degradation in the first stage, followed by gradual stiffness degradation in the second stage, and finally rapid degradation in the third stage leading to failure. The majority of the stiffness loss occurred during the first stage for all samples tested, regardless of the maximum applied stress magnitude. The rate of stiffness degradation during the second stage increased with increasing maximum stress. For the samples cycled to failure, the final stage of rapid

stiffness degradation occurred during the last 5% of the sample life and resulted in a relatively low stiffness drop prior to failure.

Edge replications were extracted for a number of tests in an effort to track damage progression during cycling at the different maximum applied stress levels. These tests were paused at various predetermined cyclic intervals to extract the edge replications during a zero-load dwell. After pausing the tests, loading resumed with the same fatigue loading conditions outlined in Section 2. The motivation was to develop a relationship between damage progression and the residual stiffness of the samples. The edge replication results for all maximum applied stress levels revealed that similar to the static tests, braider yarn cracking was the dominant damage mechanism. These cracks were distributed throughout all braider yarns across the sample width and thickness, and along the length of the samples. Most braider yarns contained multiple cracks for all maximum applied stress levels. In addition, significantly more braider yarn interface cracks were observed when compared to the static test specimens, although there were few interface cracks in comparison to the number of braider yarn cracks observed. For all maximum applied stress levels, braider yarn cracks initiated and propagated along the braider yarn axes in the first stage of cycling beginning from the first cycle, eventually reaching saturation. The rate of braider yarn crack development in this early stage of cycling increased as the maximum applied stress increased. During the initial stage of cycling, a number of localized interface cracks developed between adjacent braider yarns and at the braider yarn and 0˚ yarn interfaces. Once braider yarn crack saturation was attained, these localized interface cracks began to propagate, becoming significantly longer and interacting with each other and the braider yarn cracks by the later stages of cycling. This can be partially attributed to the shear deformation that occurred at the braider yarn interlace locations and to the straightening of the 0˚ yarns, which would cause these interface cracks to propagate under higher localized stress fields. Once the interface and braider yarn crack interaction reached a critical density, the braider yarns lost some of their load carrying capability and load was redistributed to the 0˚ yarns. As cycling continued during this final stage, splitting type cracks began to develop in the 0˚ yarns (which did not develop earlier in cycling) and fibers breaking initiated which lead to rapid failure of the sample. Like the dynamic stiffness evolution, damage development was observed to occur in three distinct stages. SEM photomicrographs obtained of sectioned samples showing the discussed damage states are shown in Figure 5.

The evolving interface cracks and their interactions ultimately lead to load redistribution and sample failure, however the initial stage of cycling was dominated by the braider yarn crack development. Figure 6 (a) and (b) show combined plots of the braider yarn crack density obtained from the edge replications and the dynamic stiffness degradation for 50% UTS and 70% UTS maximum applied stress cyclic tests, respectively. The saturation of the braider yarn cracks corresponds to the initiation of the second stage of the stiffness degradation profile for all tested specimens. This suggests that the braider yarn cracks are the main cause of rapid stiffness degradation during the initial stage of cycling. This is demonstrated by the plot of the normalized stiffness and the braider yarn crack density in Figure 6 (c), which shows that the stiffness is proportional to the braider yarn crack density up until braider yarn crack saturation. Note that each data point in the plot corresponds to a particular loading cycle. A notable difference does however exist between specimens cycled at maximum applied stresses below 60% UTS (i.e., the specimens that did not fail after run-off), and those that failed at higher stress levels. The stiffness degradation rate during the second stage was notably higher in magnitude for the specimens cycled at higher stress levels, which ultimately caused these specimens to fail (see Figure 6 (b)). It is also interesting to note that the samples

cycled at stress levels below the static transition stress of ~63% UTS did not fail, while the samples cycled at stresses >63% UTS eventually failed. There is clearly advanced damage progression during the second stage of cycling for the specimens cycled with maximum applied stresses greater than this "critical stress level". Consideration of the plot in Figure 2 (a) implies that the braider yarn density should be higher for samples cycled above the critical stress level, which in fact was found with all tested samples (e.g., compare crack density plots of Figure 6 (a) and (b)). This leads to the conclusion that since the braider yarn crack density was notably higher for the samples cycled with maximum applied stresses greater than the critical stress, the rate of the observed interface crack evolution during the second stage of cycling was higher. This is the cause of the higher magnitude stiffness degradation rate during the second stage of cycling, which ultimately lead to sample failure. Therefore, interface crack growth and the corresponding crack interactions are the main causes of stiffness degradation during the second stage of cycling.

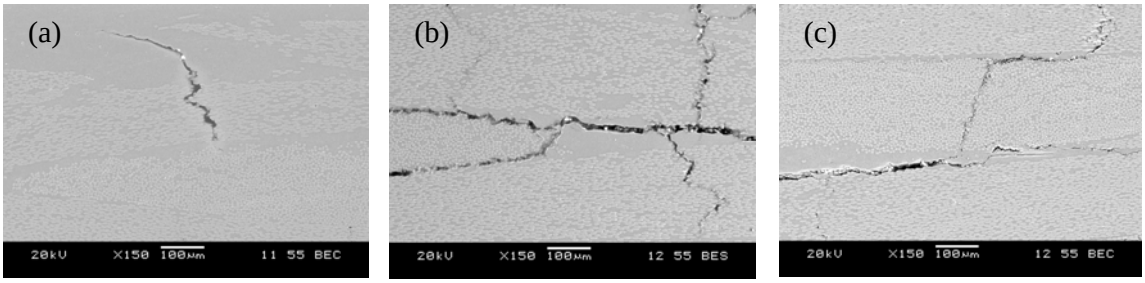

Figure 5. SEM photomicrographs illustrating (a) a braider yarn crack arrested at a 0˚ fiber yarn during the early stages of cycling, (b) - (c) crack interaction and splitting in a 0˚ yarn during the later stages of cycling.

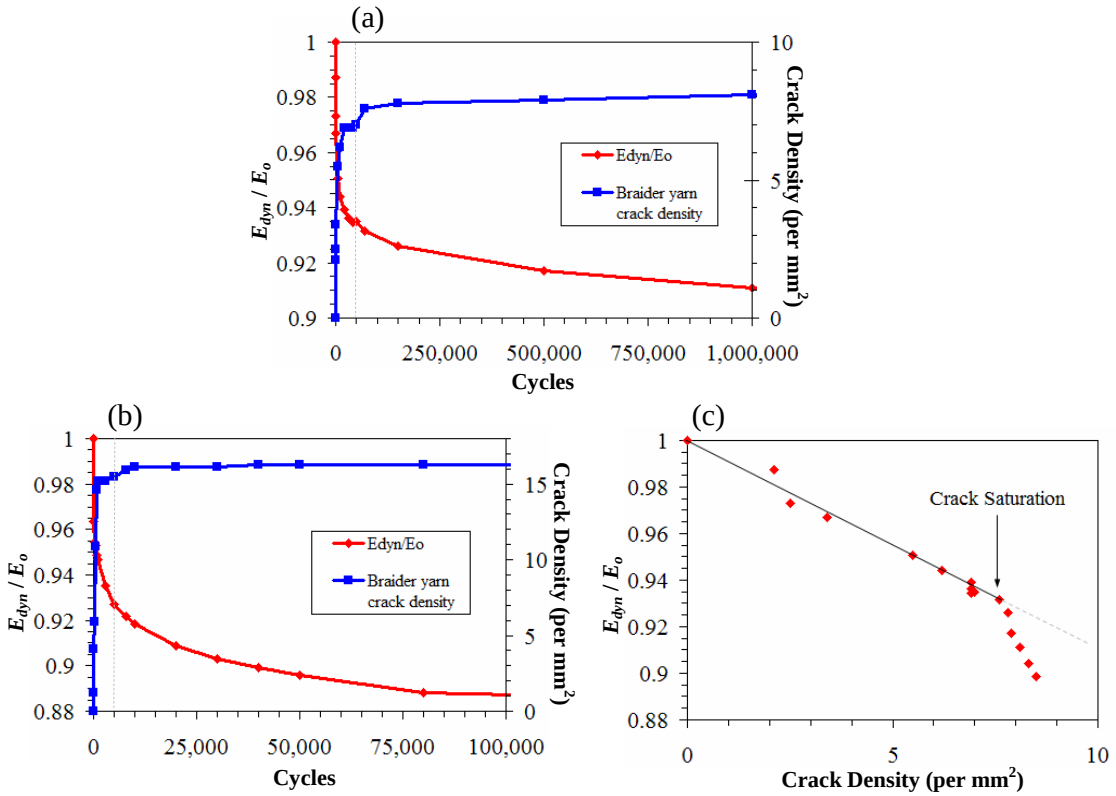

Figure 6. Stiffness degradation and crack density for maximum applied stress of (a) 50% UTS, (b) 70% UTS; (c) Stiffness versus braider yarn crack density for 50% UTS specimen.

4 Analytical fatigue damage model

As shown, cyclic loading causes the braided composite to develop irreversible damage which was directly correlated to the exhibited material behaviour. An analytical fatigue damage model would be suitable for predicting damage accumulation, providing a cost efficient method to predict the fatigue life. A number of analytical fatigue damage accumulation models have been developed for various polymeric composites [7], [8]. Due to the observed nonlinear fatigue damage behaviour and the corresponding stiffness degradation of the braided composite material, a nonlinear analytical fatigue damage model was developed with the aim of quantitatively defining a corresponding damage index. The nonlinear model used to define the damage index, *D*, is an extension of the model developed by Lemaitre and Plumtree [7], and is defined by Equation 2.

$$D = 1 - \left[1 - \left(\frac{n}{N_f} \right)^b \right]^c \tag{2}$$

The number of cycles, *n*, is normalized by the fatigue life, N_f, where the parameters *b* and *c* are material constants. It can be shown that these material constants are related by the linear relation defined in Equation 3, where constant *b* is a function of the ratio of applied maximum stress to the ultimate tensile stress, S_{max}/S_u, and defined by Equation 4.

$$c = m_1 b + m_2 \tag{3}$$

$$b = n_1 \left(\frac{S_{\max}}{S_u} \right)^{n_2} \tag{4}$$

In order to define the material constants, Equation 2 must be used to perform a regression on a suitable damage index that is based on experimental data. The damage model parameters can be defined by use of the evolving dynamic stiffness measured from the experiments. A common definition for the stiffness-based damage index is defined by Equation 5.

$$D = \frac{E_o - E_{dyn}}{E_o - E_f} \tag{5}$$

The initial stiffness, E_o, is the stiffness of the specimen prior to cycling, the dynamic stiffness, E_{dyn}, is determined from the corresponding cycle hysteretic data, and E_f is the material stiffness at failure. For the braided material of this study, the constants of Equations 3 and 4, m_1, m_2, n_1 and n_2, were found to be 4.39, 0.31, 0.033 and -1.29 respectively. Therefore, Equation 2 can be used to determine cycle-based damage progression for any maximum applied stress in conjunction with Equation 1, which is used to determine the appropriate number of cycles to failure. The corresponding model predictions results compared with the experimental results is shown in Figure 7 (a) and (b) for samples cycled with maximum applied stresses of 65% UTS and 70% UTS, respectively. The model prediction is in excellent agreement with the experimental data, based on the regression correlation factors (R^2).

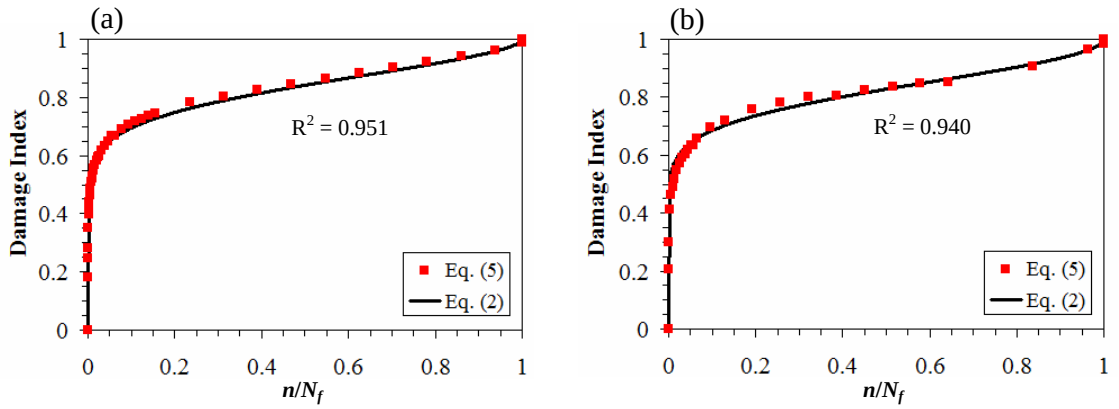

Figure 7. Experimental and predicted damage index plots (a) 65% UTS, (b) 70% UTS.

5 Conclusion

The objective of this study was to characterize the fatigue damage development of a tri-axially braided polymeric composite material. The use of edge replications and post mortem microscopic observations assisted in defining the dominant damage modes and the development of these microscopic mechanisms. Braider yarn crack development was directly correlated with the stiffness degradation of the test samples. A corresponding analytical fatigue damage model was presented to predict the damage accumulation index, which provided excellent agreement with the experimental results. The subsequent phase of model development will aim at correlating the damage model parameters with the evolving braider yarn and interface crack densities.

References

[1] Mouritz, A.P., Bannister, M.K., Falzon, P.J., Leong, K.H. Review of applications for advanced three-dimensional fibre textile composites. *Composites Part A*, **30**, pp. 1445-1461 (1999).

[2] Bannister, M.K. Development and application of advanced textile composites. *Proceedings of the Institute of Mechanical Engineers Part L - Journal of Materials*, **218**, pp. 253-260 (2004).

[3] Burr, S.T., Morris, D.H. *Two-dimensionally braided composites subjected to static and fatigue loading* in "Proceedings of *Mechanics of Textile Composites Conference*", Virginia Polytechnic Institute and State University, USA, pp. 33-53 (N96-25071 09-24) (1995).

[4] Portanova, M.A., Deaton, J.W. *Impact and Fatigue Resistance of a [±30°/0°] 3-D Braided Carbon Epoxy Composite* in "Composite Materials: Fatigue and Fracture", edited by Martin, R.H. ASTM International, Philadelphia, **STP 1230**, pp. 368-388 (1995).

[5] ASTM D 3479. *Standard Test Method for Tension-Tension Fatigue of Polymer Matrix Composite Materials* (2007).

[6] Herakovich, C.T. *Mechanics of Fibrous Composites*. John Wiley and Sons Inc., New York (1998).

[7] Lemaitre, J., Plumtree, A. Application of damage concepts to predict creep-fatigue failures. *Journal of Engineering Materials and Technology*, **101**, pp. 284-292 (1979).

[8] Mao, H., Mahadevan, S. Fatigue damage modelling of composite materials. *Composite Structures*, **58**, pp. 405-410 (2002).